Journal of Applied Fluid Mechanics, Vol. 16, No. 8, pp. 1601-1614, 2023.
Available online at www.jafmonline.net, ISSN 1735-3572, EISSN 1735-3645.
https://doi.org/10.47176/jafm.16.08.1552

Numerical Simulation of Blood Flow in Aortoiliac Bifurcation with Increasing Degree of Stenosis

J. Harris, A. Paul and B. Ghosh†

Sam Higginbottom University of Agriculture, Technology and Sciences, Prayagraj, Uttar Pradesh, 211007, India

†*Corresponding Author Email: bhavna.singh@shiats.edu.in*

ABSTRACT

The worldwide lethal prevalence of atherosclerotic diseases has made it a crucial topic of research, the descending aorta is a major artery with complex geometry involving curvature, branches, and bifurcation leading to common iliac arteries. This paper aims to scrutinize the intricate blood flow patterns and the flow parameters with the increasing degree of stenosis in the infrarenal aorta, which has been accomplished through computational fluid dynamics modeling. A 3D CAD model of the healthy aortoiliac bifurcation was constructed from MR images, and three diseased models with 32%, 47%, and 71% occlusion in the infrarenal aorta region were constructed. At the inlet, pulsatile velocity and at the outlet pressure boundary conditions were applied, blood was considered Newtonian and turbulence was modeled using Large Eddy Simulation (LES). The numerical simulation was carried out using finite volume method on ANSYS. The predicted hemodynamic parameters like velocity, wall shear stress (WSS), oscillating shear index (OSI), Q-Criterion and turbulence intensity were post-processed for all the models, the analysis of which provides an insight into the myriad processes involved in the inception and evolution of atherosclerosis. The transition of blood flow from laminar to turbulent with increase in the degree of stenosis is a very eminent feature of this study, turbulence is identified in cases with 47%, and 71% occlusion and is dominant in the latter.

Article History

Received September 11, 2022
Revised March 2, 2023
Accepted March 31, 2023
Available online May 31, 2023

Keywords:

CFD
LES
WSS
OSI
Jet

1. INTRODUCTION

In recent decades cardiovascular diseases have been ranked in the top 10 lethal diseases worldwide Roth et al. (2020) and the burden of peripheral arterial diseases (PAD) has been on an increase globally Eid et al. (2021). Cardiovascular diseases pertain to diseases of the circulatory system, namely coronary heart disease, rheumatic heart disease, congenital heart disease, cerebrovascular disease, peripheral arterial disease, pulmonary embolism and deep vein thrombosis Leong et al. (2017). Being a major underlying cause of cardiovascular diseases, atherosclerosis cuts down life years and deteriorates the quality of life. Hence, extensive studies and research providing deeper knowledge of the factors and processes involved in the genesis and evolution of atherosclerosis are needed.

Atherosclerosis, the intrinsic cause of stenosis, is an immunoinflammatory multifocal disease of the medium and large sized arteries, developing over a long period Ross (1999), Libby et al. (2002). Smoking, hyperlipidemia, diabetes mellitus, obesity, hypertension, consumption of alcohol, race, ethnicity, chronic kidney disease, inflammatory markers and hyperhomocysteinemia are significant risk factors of atherosclerosis. Sudden changes in the arterial geometry at bifurcations give rise to changes in the blood flow patterns, this further impacts the hemodynamic parameters such as wall shear stress. Low and oscillating shear stress plays a major role in the initiation of atherosclerosis, hence, favoring the development of vascular diseases at bifurcations. The study of carotid Azar et al. (2019), Gong et al. (2021) and coronary Kashyap et al. (2020); Zhao et al. (2019) artery atherosclerosis has been the centre of attention for the past decades. Peripheral arterial diseases do not pose a direct life-threatening risk but in the course of time wreaks havoc on the health of individuals. The presence of atherosclerosis in one or multiple regions of the distal abdominal aorta, femoropopliteal artery and iliac arteries is classified as Leriche Syndrome, also referred as aortoiliac occlusive disease (AIOD), which is a part of the broad spectrum of PAD. The symptomatic AIOD is indicated by the triad consisting of claudication, impotence and decrease or

Nomenclature

ρ	fluid density	$\overline{p}$	filtered pressure
μ_t	subgrid-scale eddy viscosity	Δ_f	filter-size
α	Womersley number	σ_{ij}	stress tensor
u_i	instantaneous filtered velocity component in the i direction	k_{sgs}	subgrid-scale kinetic energy
τ_{ij}	subgrid stress		

absence of femoral pulse (Wooten et al., 2014; Mohamed et al., 2021; Adnor et al., 2022).

Clinical diagnostic methods for atherosclerosis are magnetic resonance angiography, digital subtraction angiography and computed tomography angiography, these imaging techniques exhibit the vascular morphological changes caused due to atherosclerosis Kim et al. (2022). The pathophysiology of atherosclerosis is very complicated, comprehension of the varying anatomy of the human circulatory system, and the variation of the hemodynamic and biomechanical forces providing new insights into the phenomenon are required for the development of patient-specific treatment strategies.

Computational fluid dynamics can predict blood flows and biomechanical processes by mathematical modeling, numerical methods and software tools. Computer simulation offers a virtual flow laboratory where in vivo experiments can be replicated with additional predictions about the initiation of the disease. CFD provides an insight into complex flow patterns that are otherwise arduous, expensive, or even impossible to study.

Carneiro et al. (2008) implemented Newtonian and non-Newtonian models of blood flow in the idealized geometry of abdominal aorta bifurcation comparing WSS, velocity profile and recirculation zones for both cases. Barber (2017) conducted the computational simulation of a femoral artery with stenosis employing an idealised geometry. Axial flow velocity and temporal study of WSS were used to interpret the near wall parameters like OSI and residence time. Khader et al. (2018) investigated the flow field along with flow parameters like WSS and pressure in idealistic models of abdominal aorta with stenotic condition in the renal branches. Andayesh et al. (2020) investigated the effects of the geometry of renal artery and stenosis, taking into consideration the pressure regulation mechanism. Qin et al. (2021) modeled pulsatile flow of blood in the abdominal aorta including its branches which supply blood to the vital organs in the abdominal cavity; a two-level method was introduced to calculate the resistances at the outlet boundary conditions. Carvalho et al. (2021) simulated blood flow using the k −ε model in simplified and realistic aorta-iliac bifurcation models; flow patterns were investigated with reference to recirculation zones, velocity and WSS distribution in the geometries.

In the literature reviewing process, the authors did not come across any numerical simulation study based on stenosis in the distal aorta portion. This paper presents a CFD study of the blood flow in the abdominal aorta bifurcating into the iliac arteries, also known as the aortoiliac bifurcation. Four models were involved in the study; model 1 represents healthy conditions with no stenosis followed by three models with increasing degrees of stenosis representing a gradual increase in occlusion. The asymptomatic nature of atherosclerosis makes it hard to diagnose in the initial stages, hence, tools for prediction and early detection are necessary. By recognizing the precursors and indications of vascular pathologies, immediate medical attention can be sought, sparing irreversible damage and life-threatening conditions. Thus, model 1 has been considered as the base model, and alterations in the study parameters of the diseased models are meticulously inspected. The changes in the flow patterns and parameters with the change in geometry are analysed and further discussed in relation to their role in the progression of the pathology. The development of complex flow patterns and the transition of blood flow from laminar to turbulent are some prominent features of this study.

2. METHODOLOGY

The algorithm for computational modeling of the cardiovascular system initially requires the selection of the anatomical geometry and construction of the computer-aided 3D model. Previously, computational studies have been including idealized models, lately, more studies are focusing on patient-specific and realistic models as they give a better insight into real-life situations and prove to be more helpful in the development of medical strategies.

2.1. Geometry and Mesh

Considering that the geometry of the aorta involves curvature and lies in multiple planes, we have constructed four realistic 3D models of the aortoiliac bifurcation. Model 1 representing the healthy vasculature was created from MR images of 67yrs old healthy male obtained from Simtk.org in DICOM format Wilson et al. (2013). Models 2, 3 and 4 were created from model 1 representing axisymmetric development of atherosclerotic plaque in the infrarenal aorta region with 32%, 47%, and 71% decrease in diameter, respectively. The software package SimVascular was used for the segmentation and generation of 3D models**.** The models were refined of all the interferences on their surface and made suitable for meshing. The three-dimensional models with the inlet and outlet boundaries are shown in Fig. 1(a), (b), (c) and (d).

The meshing of models was done on ANSYS2022. The surface mesh for all the models was generated with minimum size 0.01, maximum size 0.3 and growth rate

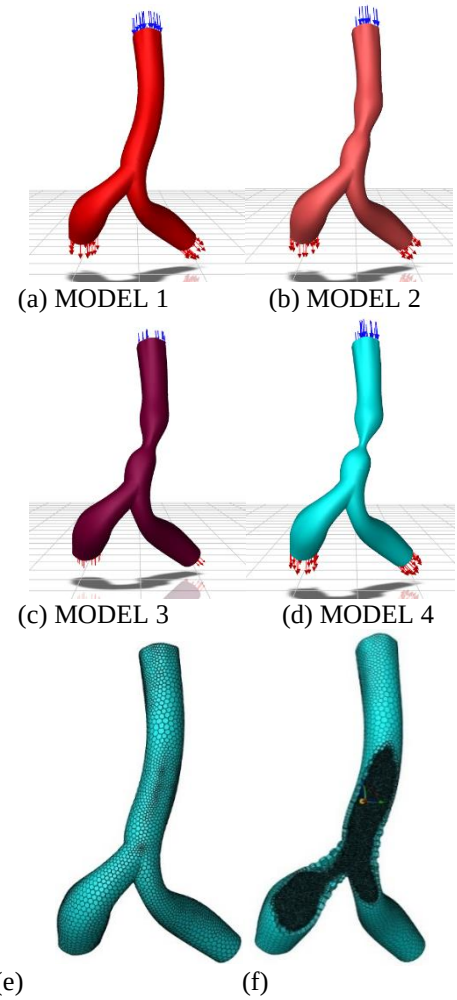

(a) MODEL 1 (b) MODEL 2

(c) MODEL 3 (d) MODEL 4

(e) (f)

Fig. 1 (a),(b),(c),(d): Models indicating inlet and outlet boundaries(e), (f): Polyhedral mesh of Model 1.

1.2. After Surface meshing, the model consists of fluid region with no voids. For refining the mesh near the walls, inlet and outlet faces three boundary layers were added at the boundary with transition ratio 0.272 and growth rate 1.2. Polyhedral cells were used owing to their superiority in terms of better convergence and higher accuracy. The spatial refinement study was carried out for Model 4 with the number of elements ranging from 30363 to 510146. The mesh with 439540 cells was found to be optimal in terms of accuracy and cost. The volumetric mesh was generated with polyhedral elements with growth rate 1.2, maximum cell length 0.05 resulting in 467515 cells for model 1, 454337 cells for model 2, 446267 cells for model 3 and 439540 cells for model 4. The mesh quality check was run and poor quality cells which comprised only 0.10% of the total mesh were improved. The vessel wall has been considered rigid and stationary; the effect of wall vibrations on the flow patterns of blood has not been considered.

a. Mathematical Model

The descending aorta starting from the aortic arch to the T4 vertebrae is the largest artery in the human anatomy, both in length and diameter, thus, making it adequate for assuming the flow of blood to be Newtonian Carneiro et al. (2008), unsteady, turbulent and incompressible. Blood density and viscosity were assumed to be 1060 kg/m^3 and 0.004 kg/(ms). This work is based on the LES approach with Dynamic Kinetic Energy Subgrid-Scale Model. The flow is governed by the filtered equations of conservation of mass and momentum (1) and (2), respectively Pope (2000). The Subgrid-Scale kinetic energy is acquired by its transport equation (3) Kim et al. (1997).

$$\frac{\partial \rho}{\partial t} + \frac{\partial}{\partial x_i}(\rho \overline{u_i}) = 0 \tag{1}$$

$$\frac{\partial}{\partial t}(\rho \overline{u_i}) + \frac{\partial}{\partial x_j}\left(\rho \overline{u_i u_j}\right) = \frac{\partial}{\partial x_j}(\sigma_{ij}) - \frac{\partial \overline{p}}{\partial x_i} - \frac{\partial \tau_{ij}}{\partial x_j} \tag{2}$$

where, i and j = 1,2 and 3 correspond to the x, y, and z coordinates, ρ fluid density, $\overline{u_i}$ is the instantaneous filtered velocity component in the i direction, σ_{ij} is the stress tensor, τ_{ij} is the subgrid stress and $\overline{p}$ is the filtered pressure.

$$\rho \frac{\partial \overline{k_{sgs}}}{\partial t} + \rho \frac{\partial \overline{u_j} \overline{k_{sgs}}}{\partial x_j} = -\tau_{ij} \frac{\partial \overline{u_i}}{\partial x_j} - C_\epsilon \rho \frac{k_{sgs}^{\frac{3}{2}}}{\Delta_f} + \frac{\partial}{\partial x_j}\left(\frac{\mu_t}{\sigma_k} \frac{\partial k_{sgs}}{\partial x_j}\right) \tag{3}$$

The subgrid-scale eddy viscosity, μ_t is given by (4) as

$$\mu_t = C_k \, \rho k_{sgs}^{1/2} \Delta_f \tag{4}$$

where C_ϵ and C_k are the model constants determined dynamically and Δ_f is the filter-size.

b. Boundary Conditions

At the aorta inlet a pulsatile velocity profile, mathematically as given by Eq. (5), is applied by a user-defined function, and at the left and right iliac outlets constant pressure of 13332 Pa is applied Sinnott et al. (2006). The wall is assumed to be stationary with no-slip condition.

$$v(t) = \begin{cases} 0.5sin[4\pi(t + 0.0160236)] \\ if\ 0.5n < x \leq 0.5n + 0.218 \\ 0.1 \quad if\ 0.5n + 0.21 < x \leq 0.5(n+1) \end{cases}$$

$$n = 0, 1, 2, 3 \ldots \tag{5}$$

c. Numerical Solution

The finite volume method based software package ANSYS was used to carry out the transient simulations. Ansys Fluent employs a control-volume based method for the numerical solution of the equation of continuity, momentum conservation equation and turbulence Versteeg and Malalasekera (2007). The conservation of each variable was guaranteed for each cell by integrating every equation over the control volume. Precisely, the differential equations result in a set of algebraic equations over the total fluid volume, the coefficient matrix of the algebraic equations was solved by Gauss-Seidel point implicit linear equation solver by Ansys Fluent. The Second Order scheme was used for solving the pressure equation, Bounded Central Differencing scheme for discretizing the momentum and Second Order Upwind discretization scheme for Subgrid kinetic energy. The fluid flow equations were resolved by using the segregated solver with the Semi-Implicit Method for Pressure Linked Equations (SIMPLE) algorithm. The equations were

Fig. 2.4. (a): 3D Idealized geometry with 75% stenosis.

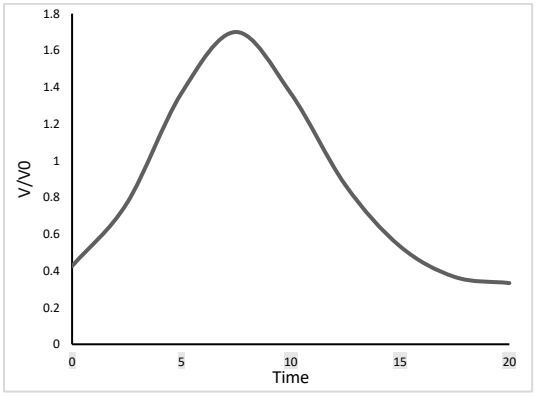

Fig. 2.4. (b): Inlet velocity

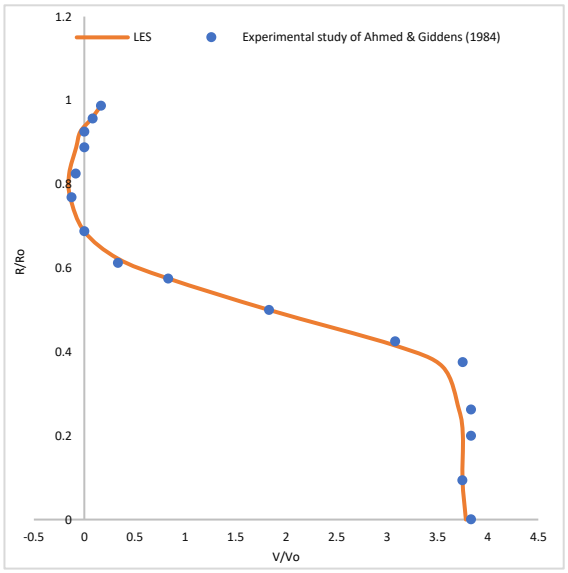

Fig. 2.4. (c): Velocity along the radius at distance 1D distal to the stenosis.

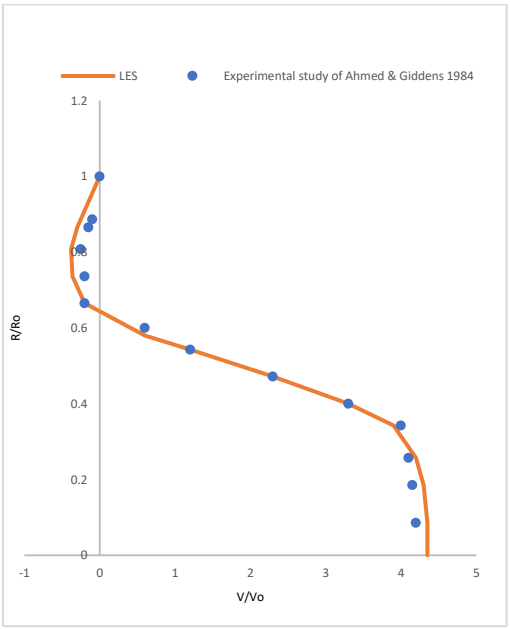

Fig. 2.4. (d): Velocity along the radius at distance 1.5 D distal to the stenosis

Table 1 Parameter values taken for the validation.

blood density	1,000 kg/m^3
dynamic viscosity	0.0036014 kg/ms
Mean velocity V_0	0.04254 m/s
Mean Reynolds number	600
Womersley number α	7.5

solved sequentially and the solution was obtained iteratively, the process was continued until the desired convergence was achieved. The convergence criteria was set at continuity, velocity and turbulence residuals < 10^{-5}.

d. Validation

For validating the present study with the experimental study of Ahmed and Giddens (1984), a 3D idealized geometry with 75% axisymmetric constriction as shown in Fig. 2.4.(a) was constructed. At the inlet, velocity profile as shown in Fig 2.4(b) and at the outlet pressure condition of 0 Pa were implemented. For the simulation various parameters were taken from the experimental study as given in Table 1. The velocity profiles along the radius at distance 1D and 1.5D distal to the stenosis are compared with the experimental results of Ahmed and Giddens (1984) and plotted in Fig. 2.4(c) & (d). We infer that the results are in good agreement with the experimental data, hence, validating the present study and the choice of LES alongwith Dynamic Kinetic Energy Subgrid-Scale Model.

3. RESULTS AND DISCUSSION

The emphasis of this work was on the variation of hemodynamic parameters and flow developments associated with the models of healthy and diseased aortoiliac bifurcation with increasing degree of stenosis. The hemodynamic parameters of interest calculated and analysed here are pressure, velocity magnitude, velocity vectors, velocity streamlines, Wall shear stress (WSS) and oscillating shear index (OSI). The flow velocity magnitude, direction, trajectory and patterns have been investigated by hemodynamic parameters like velocity vectors, velocity contours and streamlines. The onset of most cardiovascular diseases is governed by local hemodynamic factors; hence, cross-sectional and transverse sectional views were employed for extra focus on the sights of interest. Moreover, for better insight into

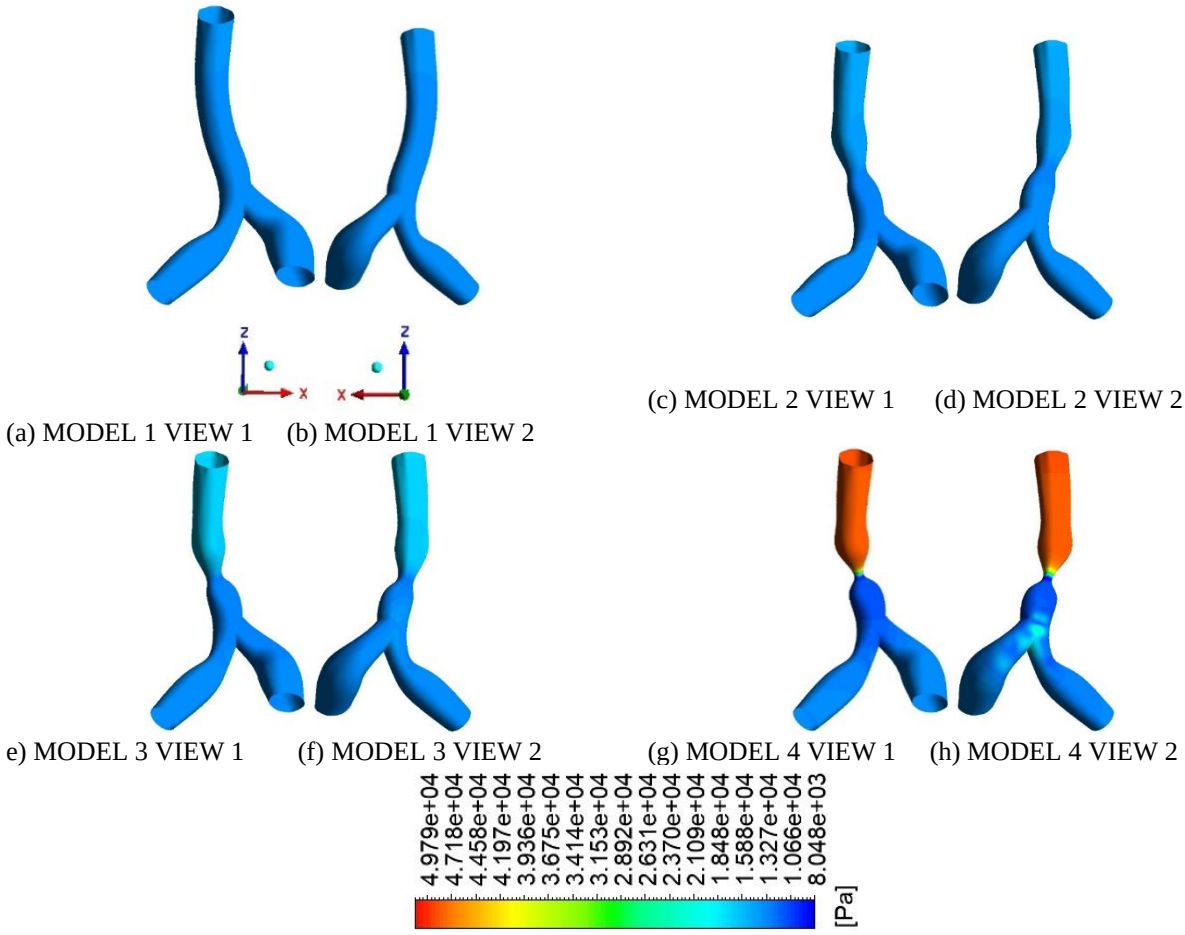

(a) MODEL 1 VIEW 1 (b) MODEL 1 VIEW 2

(c) MODEL 2 VIEW 1 (d) MODEL 2 VIEW 2

e) MODEL 3 VIEW 1 (f) MODEL 3 VIEW 2

(g) MODEL 4 VIEW 1 (h) MODEL 4 VIEW 2

Fig. 2. Pressure contours on wall

the physics of the problem the Q-Criterion, vorticity, subgrid-scale eddy viscosity and turbulence intensity were discussed.

3.1. Pressure

Pressure is the force exerted perpendicularly per unit area by the circulating blood column. Considering that the same inlet velocity and outlet pressure profiles were imposed at the boundaries, it is interesting to analyse the changing pressure patterns with the advancement of atherosclerosis radially resulting in increase in the degree of stenosis. In the healthy artery with no stenosis, the pressure on the wall takes a minor dip as blood flows from the aorta inlet to the iliac outlets because the only resistance applied is due to the geometry of the artery. As the lumen diameter decreases with atherosclerosis progression in models 2,3 and 4, the resistance increases and it is observed that the pressure drop across the geometries increases by 1.95 times, 3.91 times and 32.31 times, respectively, from that of model 1. This pressure drop is validated by Bernoulli's Equation Duncker et al. (2015). While the pre-stenotic regions exhibit an increase of 6.51%, 21.64% and 250%, respectively, in the maximum pressure range in comparison to the healthy case, the pressure in post-stenotic region decreases. Higher pressure in the pre-stenotic region is observed with abnormally high pressure values in case of severe occlusion, Fig. 2.

To assess the pressure at the sites of interest, four cut planes parallel to XY plane were set at the iliac region, throat of the stenosis, pre-stenotic and post-stenotic regions. In Fig. 3 the pressure contours at cross-sectional planes are presented and it is observed that at the throat of the stenosis, high pressure is exerted at the centre and lower pressure is exerted at the circumference because of frictional force.

a. Wall shear stress

WSS is the measure of the frictional force applied by the circulating blood column, per unit area, on the vessel wall, it plays a vital role in the development and progression of vessel wall pathologies. Regions of low and oscillating WSS, zones of blood recirculation and low velocity, create optimal conditions for plaque development, by aiding infiltration of lipids, hence, WSS is considered as a crucial factor in the localization and development of atherosclerotic plaques Cecchi et al. (2011). High wall shear stress at the regions with atherosclerotic plaque can destabilize the plaque by causing injuries to the endothelial cells, this, in turn, plays a major role in thinning of the fibrous cap which can lead to its rupture, resulting in thrombosis. Once thrombosis takes place the clotting in the bloodstream clogs the artery and hinders the supply of blood Hartman et al. (2021). The

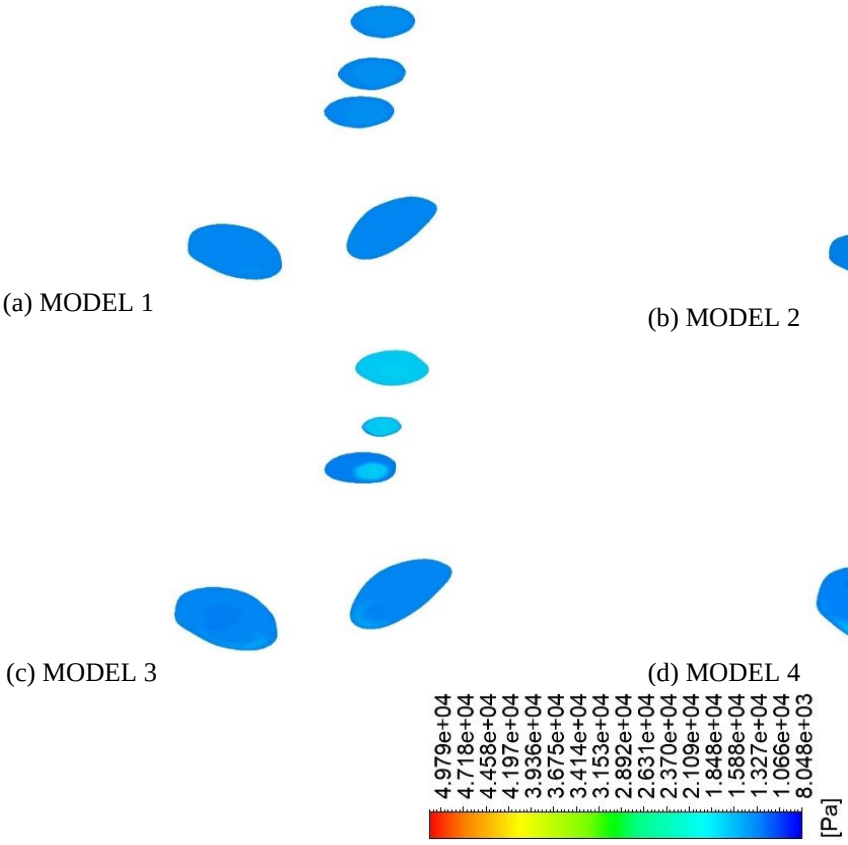

(a) MODEL 1 (b) MODEL 2

(c) MODEL 3 (d) MODEL 4

Fig. 3. Pressure contours at planes.

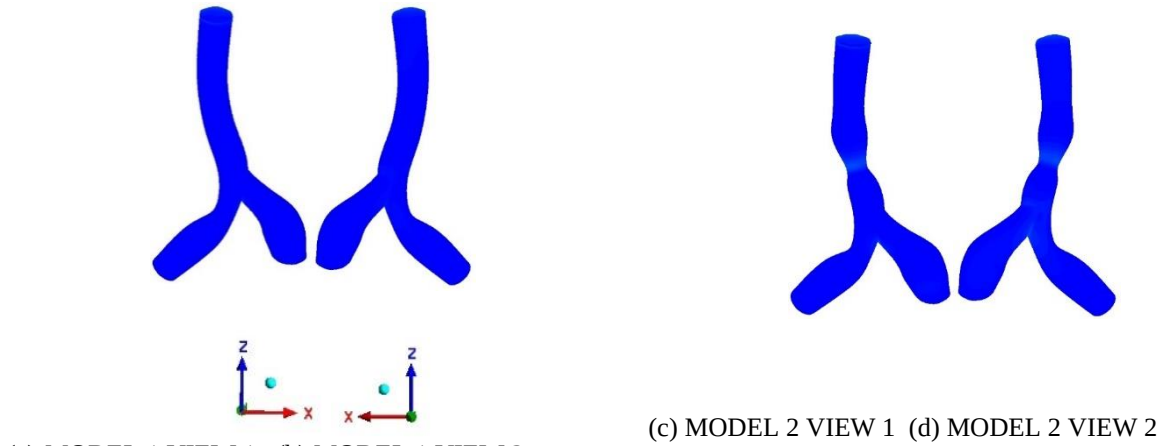

(a) MODEL 1 VIEW 1 (b) MODEL 1 VIEW 2 (c) MODEL 2 VIEW 1 (d) MODEL 2 VIEW 2

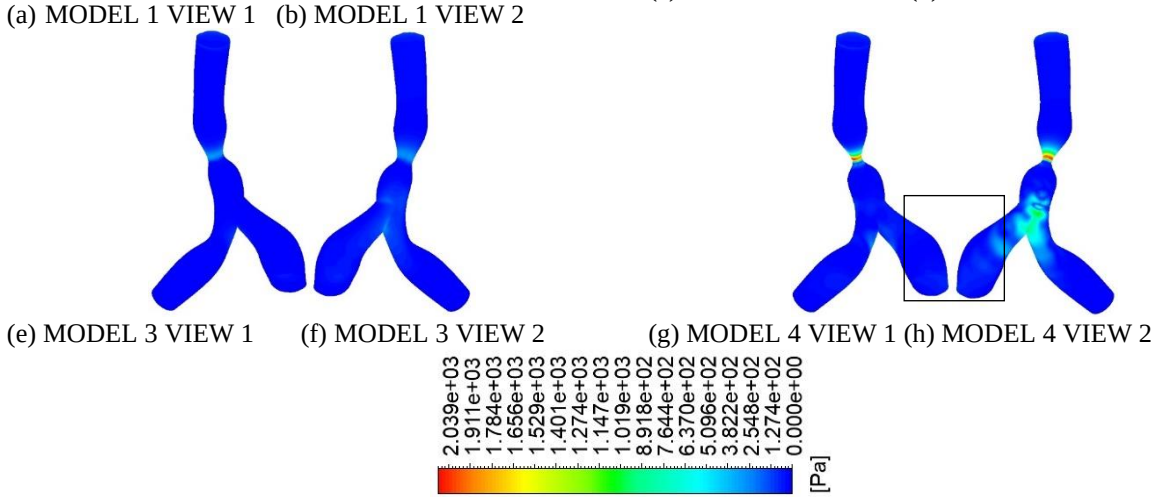

(e) MODEL 3 VIEW 1 (f) MODEL 3 VIEW 2 (g) MODEL 4 VIEW 1 (h) MODEL 4 VIEW 2

Fig. 4. Wss contours

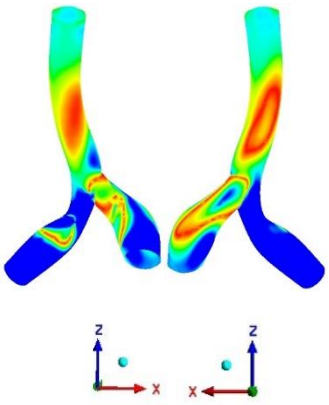

(a) MODEL 1 VIEW 1 (b) MODEL 1 VIEW 2

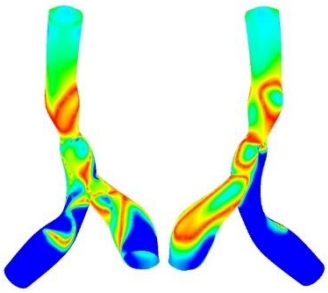

(c) MODEL 2 VIEW 1 (d) MODEL 2 VIEW 2

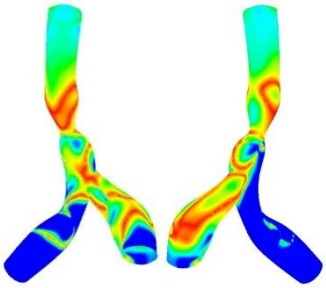

(e) MODEL 3 VIEW 1 (f) MODEL 3 VIEW 2

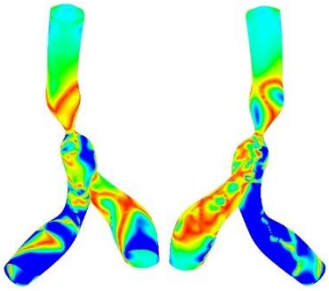

(g) MODEL 4 VIEW 1 (h) MODEL 4 VIEW 2

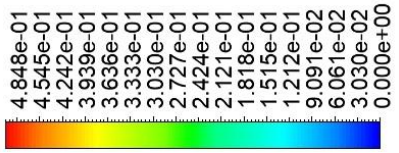

Fig. 5. Osi contours.

contours in Fig. 4 represent the distribution and the changes in WSS with increase in degree of stenosis in all four cases. At the site of atherosclerosis, WSS is increasing with the decrease in lumen diameter. In Fig. 4(h) patterns of increased WSS are also recorded around the apex of bifurcation.

b. Oscillating Shear Index

The OSI is a nondimensional WSS based hemodynamic indicator that measures the directional change in WSS during the cardiac cycle. Unidirectional WSS and fully oscillatory flow are indicated by OSI values 0.0 and 0.5, respectively, which is the range of OSI. It is calculated using Eq.(7)

$$\mathrm{OSI} = 0.5\left(1 - \frac{\left|\int_0^T WSS dt\right|}{\int_0^T |WSS| dt}\right) \tag{7}$$

A high value and large effective area of the OSI are believed to result in unexpected hemodynamic changes at the vessel wall triggering atherogenic activities led by monocyte chemotactic protein-1 (MCP-1) and platelet-derived growth factors (PDGFs) in endothelial cells. The distribution of OSI as predicted on the arterial wall is depicted by contour plots in Fig. 5. The change in geometry due to the pathology, changes OSI patterns in the vasculature and indicates an increase in the oscillatory nature of blood flow, which is a key factor in deranging endothelial cell alignment thus predicting further progression of the disease.

c. Velocity Distribution

The velocity vectors signify both direction and magnitude of velocity, they are helpful in the identification of zones of flow recirculation and vortex formation. The velocity vectors in Fig. 6 clearly show the influence of the increasing degree of stenosis on the flow downstream, especially near the wall. The change in velocity profile, magnitude and direction can be visualized at the sites of interest by setting cut planes in the cross sections as in Fig. 7. Contours of velocity magnitude are presented in Fig. 8 at the transverse plane and in Fig. 9 at three cross sectional planes (P1, P2 and P3), for all the four models.

In model 1 the fully developed flow has a parabolic velocity profile with higher centreline velocity throughout the aorta region as presented in Fig 7(a) at planes P1, P2 and P3. The velocity contours in Fig 8(a), Fig 9(a)(i), 9(b)(i) and 9(c)(i) indicate that the flow velocity in the healthy artery follows the same profile in the aorta region before flow separation begins near the apex of bifurcation. In the course of its flow in the iliac region, the velocity profile gets skewed towards the inner walls of the vessel owing to the centrifugal forces. In model 2 the flow

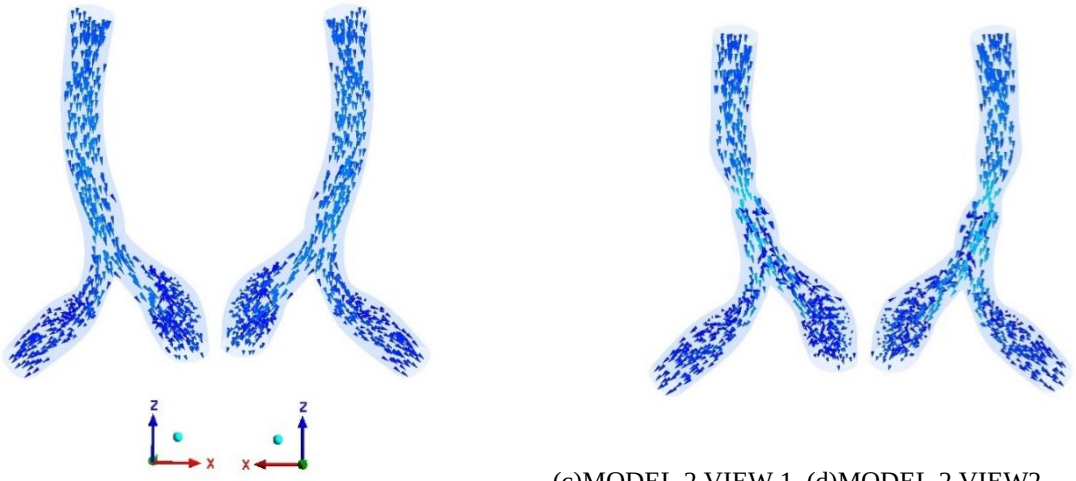

(a)MODEL 1 VIEW 1 (b) MODEL 1 VIEW 2 (c)MODEL 2 VIEW 1 (d)MODEL 2 VIEW2

(e)MODEL 3 VIEW 1 (f)MODEL 3 VIEW 2 (g)MODEL 4 VIEW 1 (h)MODEL 4 VIEW 2

Fig. 6. Velocity vectors.

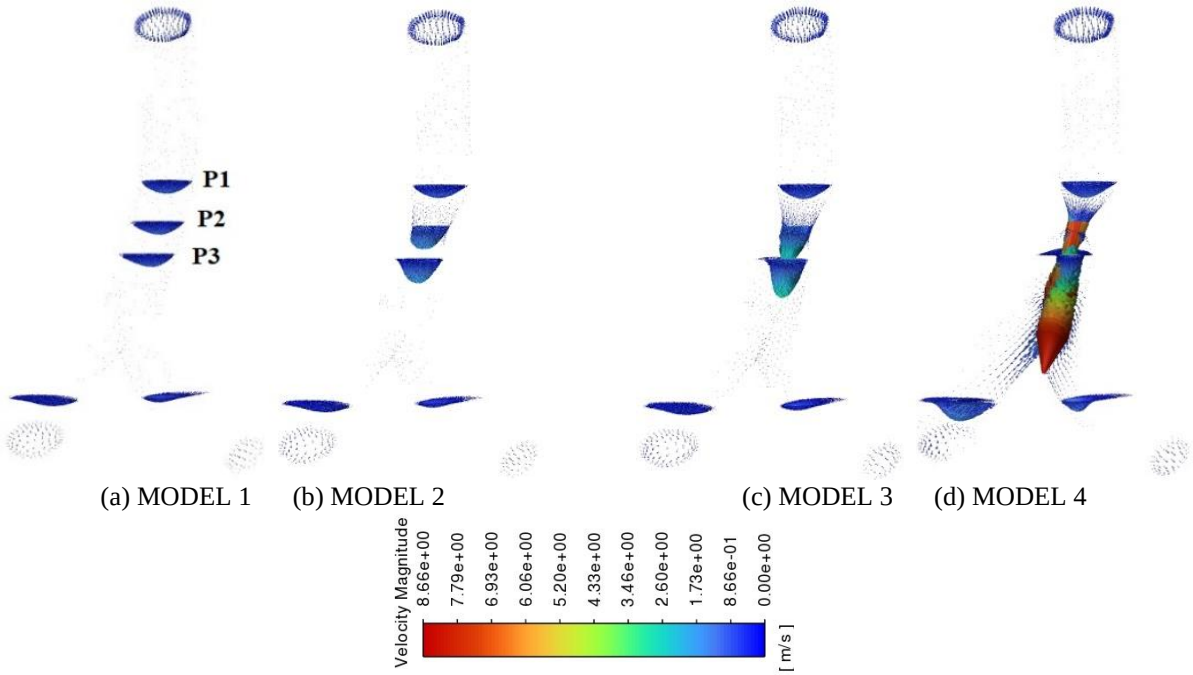

(a) MODEL 1 (b) MODEL 2 (c) MODEL 3 (d) MODEL 4

Fig. 7. Velocity vectors at cross-sectional planes.

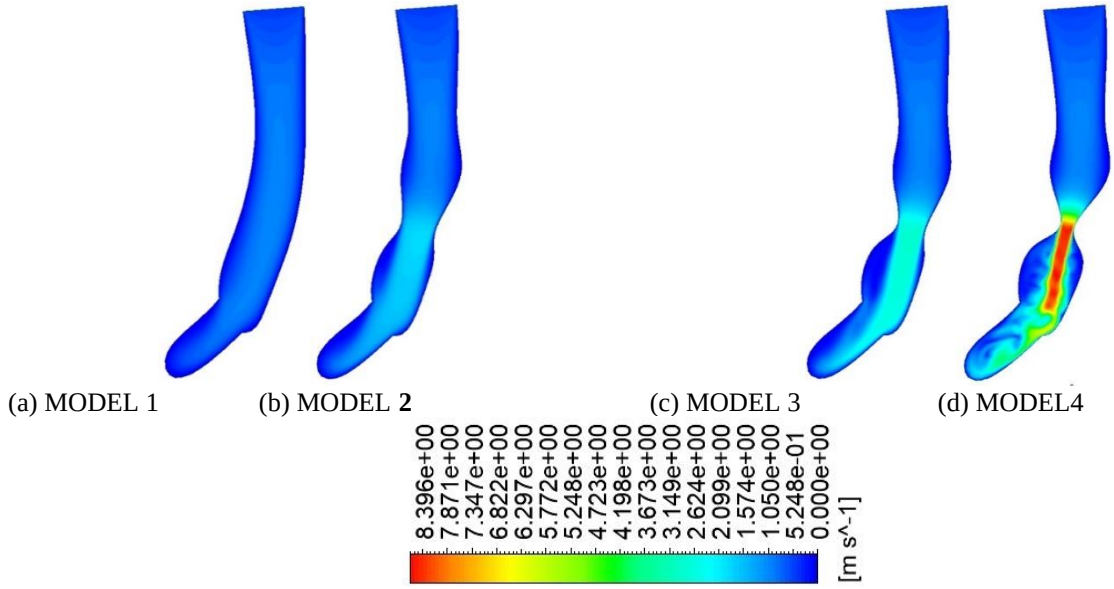

(a) MODEL 1 (b) MODEL **2** (c) MODEL 3 (d) MODEL4

Fig. 8. Velocity contours at transverse planes.

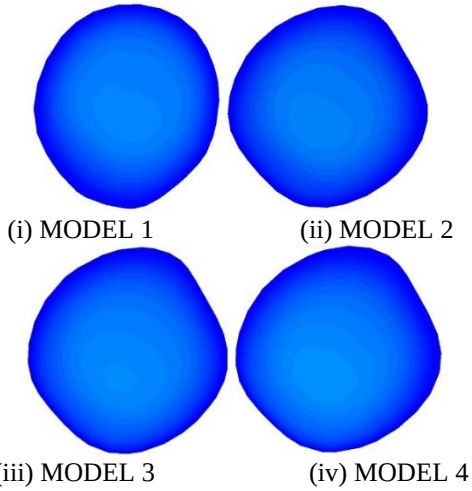

(i) MODEL 1 (ii) MODEL 2

(iii) MODEL 3 (iv) MODEL 4

Fig. 9(a) Velocity contours at plane P1.

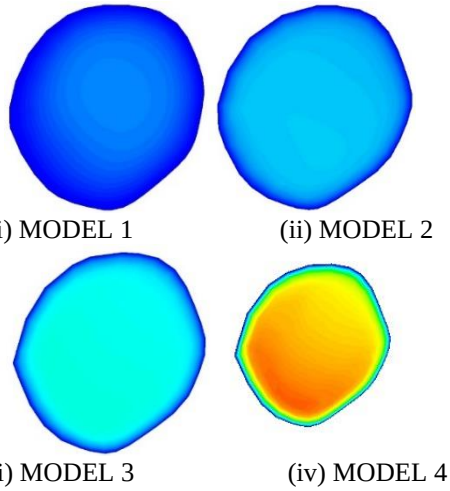

(i) MODEL 1 (ii) MODEL 2

(iii) MODEL 3 (iv) MODEL 4

Fig. 9(b) Velocity contours at plane p2.

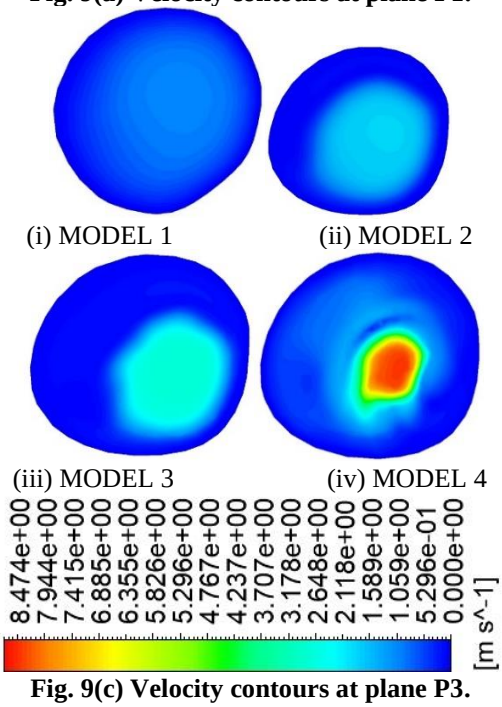

(i) MODEL 1 (ii) MODEL 2

(iii) MODEL 3 (iv) MODEL 4

Fig. 9(c) Velocity contours at plane P3.

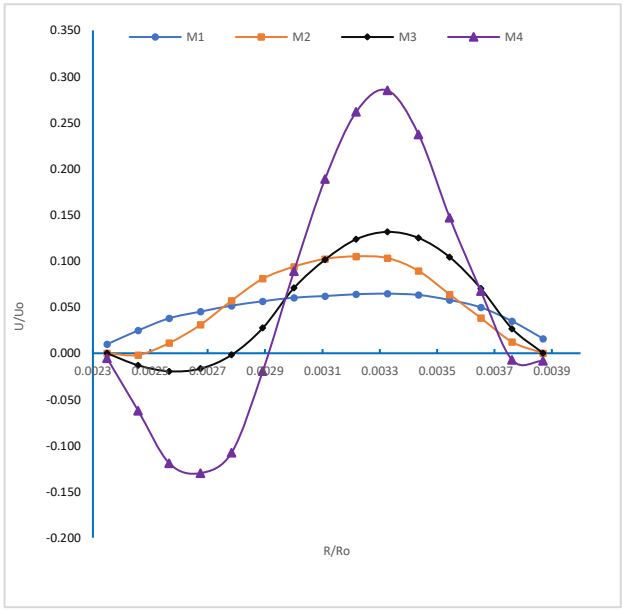

Fig. 9(d) Velocity profile at diameter of plane P3 in the post-stenotic region.

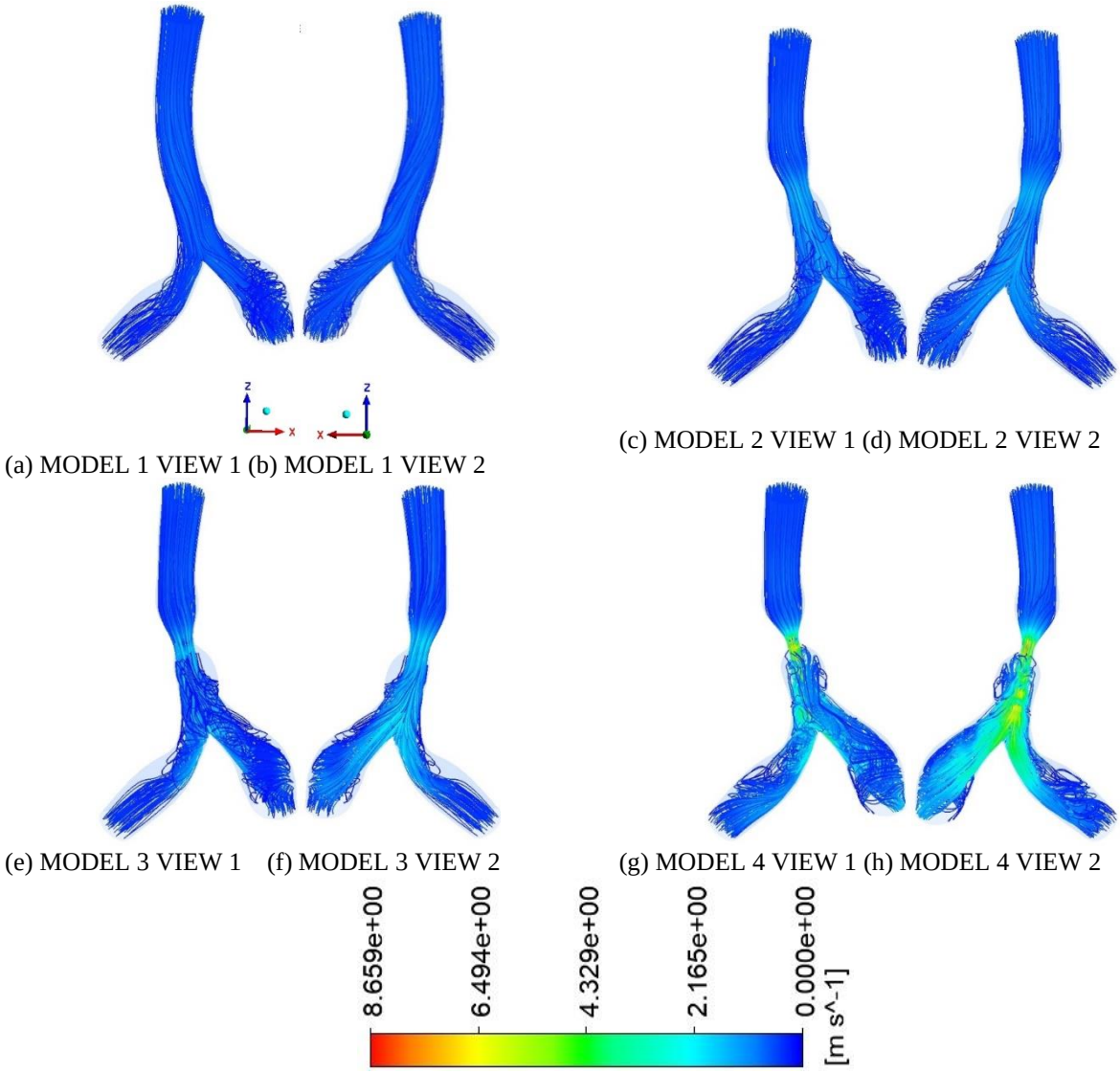

(a) MODEL 1 VIEW 1 (b) MODEL 1 VIEW 2 (c) MODEL 2 VIEW 1 (d) MODEL 2 VIEW 2

(e) MODEL 3 VIEW 1 (f) MODEL 3 VIEW 2 (g) MODEL 4 VIEW 1 (h) MODEL 4 VIEW 2

Fig. 10. Velocity streamlines.

velocity increases with the decrease in lumen area due to the presence of stenosis as seen at plane P2 in Fig 7(b) and 9(b)(ii). The velocity contours shift slightly towards the wall in Fig 9(c)(ii). Influence of mild stenosis is reflected by the change in velocity distribution but no major flow disturbance is observed.

In model 3 with 47% decrease in lumen, the flow velocity increases and noticeable changes in flow patterns are detected, Fig 9(a)(iii), 9(b)(iii) and 9(c)(iii). A separation and recirculation zone starts to develop in the post-stenotic region near the wall, (the intensity is inferred from the density and size of velocity vectors) Fig. 6(e)(f), which further amplifies and becomes fully developed in model 4, Fig 6(g)(h). The regions of recirculation imply a longer residence time of blood on the lumen wall which assists the growth of atherosclerotic plaque Zhu et al. (2018).

Moreover, with an increase in the degree of stenosis to 71% the velocity of blood flow accelerates through the throat of stenosis Fig 7(d), Fig 9(b)(iv) and decelerates in the post-stenotic region, the sudden drastic fluctuation in velocity magnitude induces jet-like flow Fig 8(d). It is also observed that the flow is directed towards the wall in the post-stenotic region giving rise to a wall jet Fig. 7(d).

In the post-stenotic region, the change in velocity profile is evident with the increasing degree of stenosis, Fig 9(d).

Velocity streamlines are tangential to the instantaneous velocity vectors. They are instrumental in flow visualization, helping in the tracking of flow trajectory and identification of flow disturbances. In Fig. 10 velocity streamlines in the aforementioned aortoiliac models are presented. In Fig. 10 (a), (b) the flow in the aortic region is laminar as suggested by regular streamlines, further the flow bifurcates into the common iliac arteries. While the flow in the right iliac can be said to be laminar, the left iliac manifests helical flow due to its curved geometry. Low intensity helical patterns mark zones of disturbed shear stress, whereas, high levels of helicity are known to restrain disruptions in blood flow Gallo et al. (2012). For 32%, 47% and 71% degree of stenosis the velocity gradient across the geometries increases by 1.86 times, 2.81 times and 8.45 times, respectively. The velocity streamlines congregate with a decrease in lumen area due to the increase in stenosis

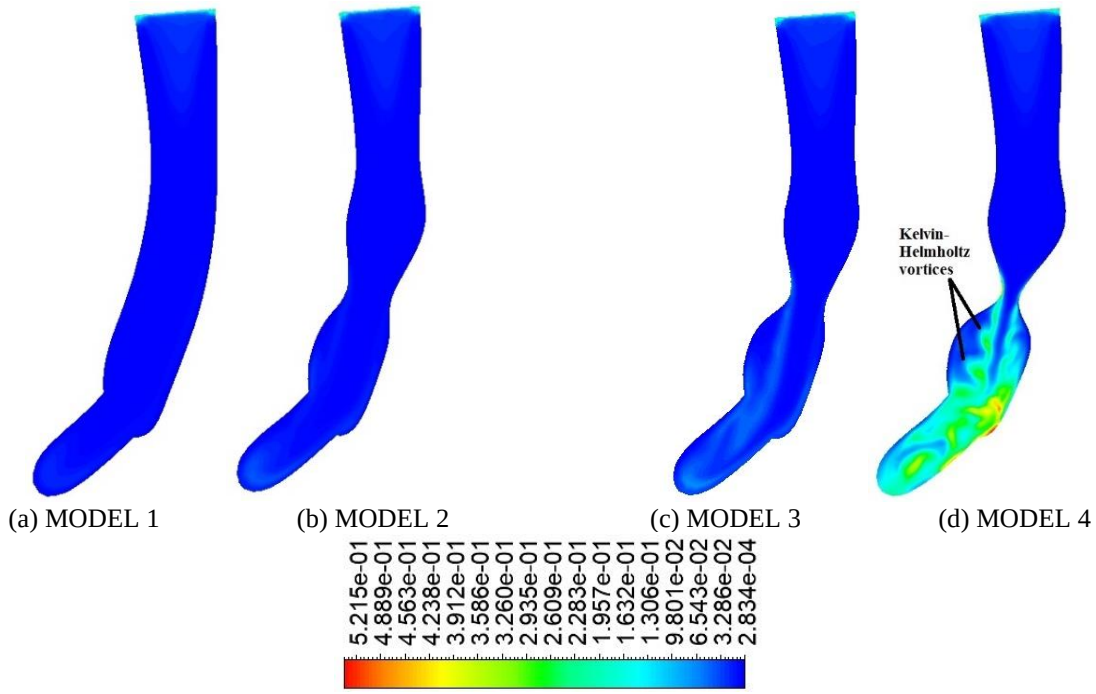

(a) MODEL 1 (b) MODEL 2 (c) MODEL 3 (d) MODEL 4

Fig. 11. Turbulence intensity.

degree and the flow attains its highest velocity at the most constricted region in each case. As blood travels across the stenosis, it is concentrated towards the centreline and inner wall of the iliac arteries, thus limiting the supply of blood to the wall. Bifurcation of flow towards the left and right common iliac can be seen clearly with the help of streamlines just before the apex of aortoiliac bifurcation. In the post-stenotic region, the helical patterns intensify, flow separation and recirculation with the development of swirling flow, characterising turbulence, is observed in Models 3 and 4. The transition of flow from laminar to turbulent is predicted with the increase in the degree of stenosis.

3.5 Transition to Turbulence

Turbulence is dominant in the post-stenotic region in Model 4 as seen in Fig 10(g) & 10(h). The main flow feature of turbulence is chaotic flow and can be easily visualised in Fig 6(g),6(h),10(g) & 10(h).

The turbulence intensity can be expressed as

$$I = \frac{\sqrt{\frac{2}{3}k}}{\overline{U}} \tag{8}$$

Where, k is kinetic energy and $\overline{U}$ is the average velocity.

The contour plots of turbulence intensity on the transverse plane are presented in Fig. 11 for each of the four models. In Fig.11 (a) and (b) the turbulence intensity is negligible. Whereas, in Fig 11(c) visible increase in turbulence intensity is noted in the post stenotic region owing to the high shear layer due to the flow with increased velocity through the stenosis. Furthermore, in Fig 11(d) regions of high turbulence intensity are present in the post stenotic region. High velocity region Fig 8(d) lying towards the inner shear layer (slip line) and lower velocity regions towards the outer shear layer (jet

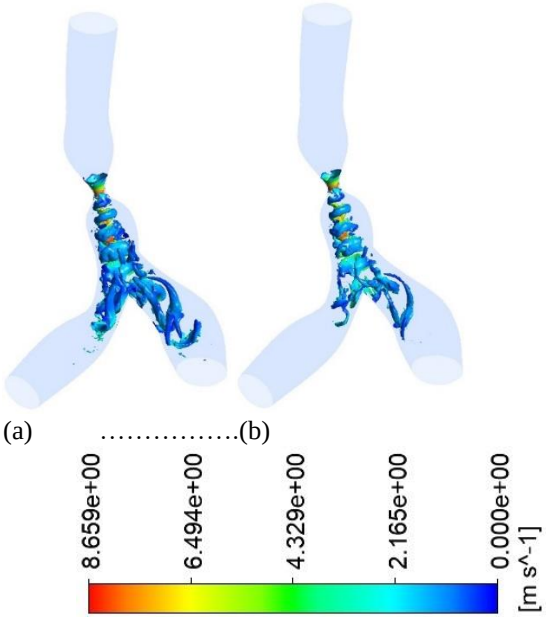

(a) …….(b)

Fig. 12. Iso-surfaces of Q-Criteria with threshold values (a) Q= 2e+07 and (b) Q= 7e+07 coloured by Velocity magnitude.

boundary) result in instability of the shear layer. As a consequence of this instability, the shear layers roll-up giving rise to Kelvin-Helmholtz vortices as marked in Fig 11(d). As the jet propogates downstream, it diverges and grows closer to the wall, hence, the Kelvin-Helmholtz rollers become imprecise.

The Q-criterion is defined as

$$Q = \frac{1}{2}(||\Omega||^2 - ||S||^2) \tag{9}$$

Where, Ω is the vorticity tensor and S is the strain rate tensor.

The vortical structures in model 4 are shown in Fig. 12(a) and (b) at Q-Criteria 2e+07 and 7e+07, respectively. The post-stenotic region in model 4 harbours a fully developed turbulent jet. The throat of the stenosis fosters the jet's core. In the initial portion of the jet four vortex rings lead by an undulating vortex ring with increasing radius are evident, due to the instability of the flow these are slightly distorted. Subsequently, bifurcation of the next vortex ring is observed at the apex of bifurcation of the artery wall Fig. 12(b). Gradually, the coannular shear layers are replaced by streamwise vortices which are embedded together; due to the 3D Kelvin-Helmholtz instabilities these coherent vortical structures rotate individually and flow downstream Fig. 12(a).

4. CONCLUSION

Using Large Eddy Simulations (LES), the effect of increasing degree of stenosis due to atherosclerotic plaque growth was studied in realistic models of a healthy and three atherosclerotic cases with 32%, 47% and 71% occlusion in the infrarenal region of aortoiliac bifurcation. The study incorporated hemodynamic parameters and WSS-based descriptor OSI for an enhanced understanding of perturbations in blood flow and atherosclerosis advancement. These parameters also partake in the prediction, detection and treatment of arterial diseases.

The pressure gradient in the geometries is seen to vary enormously due to the presence of atherosclerotic plaque. By applying one-way ANOVA pressure and velocity variation in the four models was found to be statistically significant with p values < 0.05. Elevated levels of WSS at the plaque site, new regions of low WSS and intensified oscillatory flow indicate potential plaque rupture and atherosclerosis progression. The study predicts that with further increase in the degree of stenosis, the transition of blood flow from laminar to turbulent will be intensified with very high turbulent kinetic energy in the post-stenotic region. Flow separation and vortex formation starts in Model 3 verifying the inception of turbulence. The flow separation will amplify in the region right after the stenosis along with an increase in the recirculation area Liu (2007). According to prior works including different geometries, turbulence creeps in from 50% degree of stenosis and the flow becomes fully turbulent at and above 75%. As the realistic geometries in our study take into account the curvature of the geometry it is observed that the laminar flow in the infrarenal region begins to show some turbulent features at 47% degree of stenosis and becomes fully turbulent at 71%. Ascertaining that curvature favours turbulence.

Additionally, LES provides a deep understanding of the blood flow dynamics at macro and micro scales. The turbulent features and the existence of a fully developed turbulent jet in Model 4 are thoroughly inspected.

The major assumptions in this study are rigid, stationary artery wall and axisymmetric plaque growth. Acquisition of Patient-specific data of the same geometry with varied conditions is challenging, hence, realistic geometries were used for different degrees of stenosis. As the results predict potential possibility of plaque rupture, for future studies, incorporating the multiphase flow of blood together with the hyperelastic nature of the plaque and artery wall may provide an enhanced outlook. The study can be extended by including the effect of vessel wall vibrations.

ACKNOWLEDGEMENT

The authors are grateful to the reviewers for their valuable comments which have helped in the improvement of this paper.

CONFLICT OF INTEREST

There is no conflict that authors have to disclose.

AUTHORS CONTRIBUTION

Josephina Harris: formal analysis, resources, software, visualization, writing- original draft; A. Paul: writing- review & editing, resources, validation, visualization; Bhavna Singh Ghosh: conceptualization, investigation, methodology, supervision, writing- review & editing

REFERENCES

Adnor, S., El Kourchi, M., & Wakrim, S. (2022). When the aortoiliac bifurcation is occluded: Leriche syndrome. *Annals of Medicine and Surgery*, 75, 103413. https://doi.org/10.1016/j.amsu.2022.103413

Ahmed, S. A., & Giddens, D. P. (1984). Pulsatile poststenotic flow studies with laser doppler anemometry. *Journal of Biomechanics*, 17(9), 695–705. https://doi.org/10.1016/0021-9290(84)90123-4

Andayesh, M., Shahidian, A., & Ghassemi, M. (2020). Numerical investigation of renal artery hemodynamics based on the physiological response to renal artery stenosis. *Biocybernetics and Biomedical Engineering*, 40(4), 1458–1468. http://dx.doi.org/10.1016/j.bbe.2020.08.006

Azar, D., Torres, W. M., Davis, L. A., Shaw, T., Eberth, J. F., Kolachalama, V. B., Lessner, S. M., & Shazly, T. (2019). Geometric determinants of local hemodynamics in severe carotid artery stenosis. *Computers in Biology and Medicine*, 114, 103436. https://doi.org/10.1016%2Fj.compbiomed.2019.103436

Barber, T. (2017). Wall shear stress and near-wall flows in the stenosed femoral artery. *Computer Methods in Biomechanics and Biomedical Engineering*, 20(10), 1048–1055. https://doi.org/10.1080/10255842.2017.1331342

Carneiro, F., Ribeiro, V. G., Teixeira, J., & Teixeira, S. (2008). Numerical study of blood fluid rheology in the abdominal aorta. *Design & Nature IV: Comparing Design in Nature with Science and Engineering*, 4, 169. https://doi.org/10.2495/DN080181

Carvalho, V., Carneiro, F., Ferreira, A. C., Gama, V., Teixeira, J. C., & Teixeira, S. (2021). Numerical study of the unsteady flow in simplified and realistic iliac bifurcation models. *Fluids*, 6(8), 284. https://doi.org/10.3390/fluids6080284

Cecchi, E., Giglioli, C., Valente, S., Lazzeri, C., Gensini, G. F., Abbate, R., & Mannini, L. (2011). Role of hemodynamic shear stress in cardiovascular disease. *Atherosclerosis*, 214(2), 249–256. https://doi.org/10.1016/j.atherosclerosis.2010.09.008

Duncker, D. J., Koller, A., Merkus, D., & Canty Jr, J. M. (2015). Regulation of coronary blood flow in health and ischemic heart disease. *Progress in Cardiovascular Diseases*, 57(5), 409–422. https://doi.org/10.1016/j.pcad.2014.12.002

Eid, M. A., Mehta, K., Barnes, J. A., Wanken, Z., Columbo, J. A., Goodney, P., & Mayo-Smith, M. (2021). Global burden of disease of peripheral artery disease. *Journal of Vascular Surgery*, 74(3), e255. https://doi.org/10.1016/j.jvs.2022.12.015

Gallo, D., Steinman, D. A., Bijari, P. B., & Morbiducci, U. (2012). Helical flow in carotid bifurcation as surrogate marker of exposure to disturbed shear. *Journal of biomechanics*, 45(14), 2398–2404. https://doi.org/10.1016/j.jbiomech.2012.07.007

Gong, X., Liang, Z., Wang, Y., Zhang, C., Xie, S., & Fan, Y. (2021). Comparative study on hemodynamic environments around patient-specific carotid atherosclerotic plaques with different symmetrical features. *Medicine in Novel Technology and Devices*, 11, 100079. https://doi.org/10.1016/j.medntd.2021.100079

Hartman, E. M., De Nisco, G., Gijsen, F. J., Korteland, S. A., Van der Steen, A. F., Daemen, J., & Wentzel, J. J. (2021). The definition of low wall shear stress and its effect on plaque progression estimation in human coronary arteries. *Scientific Reports*, 11(1), 1–11. https://doi.org/10.1038/s41598-021-01232-3

Kashyap, V., Arora, B., & Bhattacharjee, S. (2020). A computational study of branch-wise curvature in idealized coronary artery bifurcations. *Applications in Engineering Science*, 4, 100027. https://doi.org/10.1016/j.apples.2020.100027

Khader, S. M. A., Azriff, A., Johny, C., Pai, R., Zuber, M., Ahmad, K. A., & Ahmad, Z. (2018). Haemodynamics behaviour in normal and stenosed renal artery using computational fluid dynamics. *Journal of Advanced Research in Fluid Mechanics and Thermal Sciences*, 51(1), 80–90.

Kim, S. J., Schneider, D. J., Feldmann, E., & Liebeskind, D. S. (2022). Intracranial atherosclerosis: Review of imaging features and advances in diagnostics. *International Journal of Stroke*, 17474930211066427. https://doi.org/10.1177/17474930211066427

Kim, W. W., Menon, S., Kim, W. W., & Menon, S. (1997). *Application of the Localized Dynamic Subgrid-Scale Model to Turbulent Wall-Bounded Flows*. 35th Aerospace Sciences Meeting and Exhibit, 210. https://doi.org/10.2514/6.1997-210

Leong, D. P., Joseph, P. G., McKee, M., Anand, S. S., Teo, K. K., Schwalm, J. D., & Yusuf, S. (2017). Reducing the global burden of cardiovascular disease, part 2: prevention and treatment of cardiovascular disease. *Circulation research*, 121(6), 695–710. https://doi.org/10.1161/CIRCRESAHA.117.311849

Libby, P., Ridker, P. M., & Maseri, A. (2002). Inflammation and atherosclerosis. *Circulation*, 105(9), 1135–1143. https://doi.org/10.1161/hc0902.104353

Liu, B. (2007). The influences of stenosis on the downstream flow pattern in curved arteries. *Medical Engineering & Physics*, 29(8), 868–876. https://doi.org/10.1016/j.medengphy.2006.09.009

Mohamed, A., Mattsson, G., & Magnusson, P. (2021). A case report of acute leriche syndrome: aortoiliac occlusive disease due to embolization from left ventricular thrombus caused by myocarditis. *BMC Cardiovascular Disorders*, 21(1), 1–5. https://doi.org/10.1186/s12872-021-02031-4

Wilson, N. M., Ortiz, A. K., & Johnson, A. B. (2013). The Vascular Model Repository: A Public Resource of Medical Imaging Data and Blood Flow Simulation Results. *Journal of medical devices* 7(4), 040923. (Dec 05,2013). https://doi.org/10.1115/1.4025983.

Pope, S. B. (2000). *Turbulent flows*. Cambridge university press. https://doi.org/10.1017/CBO9780511840531

Qin, S., Chen, R., Wu, B., Shiu, W. S., & Cai, X. C. (2021). Numerical simulation of blood flows in patient-specific abdominal aorta with primary organs. *Biomechanics and Modeling in Mechanobiology*, 20(3), 909–924. https://doi.org/10.1007/s10237-021-01419-7

Ross, R. (1999). Atherosclerosis—an inflammatory disease. *New England journal of Medicine*, 340(2), 115–126. https://doi.org/10.1056/NEJM199901143400207

Roth, G. A., Mensah, G. A., Johnson, C. O., Addolorato, G., Ammirati, E., Baddour, L. M., Barengo, N. C.,Beaton, A. Z., Benjamin, E. J., Benziger, C. P., et al. (2020). Global burden of cardiovascular diseases and risk factors, 1990–2019: update from the gbd 2019 study. *Journal of the American College of Cardiology*,76(25), 2982–3021. https://www.jacc.org/doi/10.1016/j.jacc.2020.11.010

Sinnott, M., Cleary, P. W., & Prakash, M. (2006). *An Investigation of Pulsatile Blood Flow in a Bifurcation Artery Using a Grid-Free Method*. Proc. Fifth International Conference on CFD in the Process Industries.

Versteeg, H. K., & Malalasekera, W. (2007). *An introduction to computational fluid dynamics: the finite volume method*. Pearson Education.

Wooten, C., Hayat, M., Du Plessis, M., Cesmebasi, A., Koesterer, M., Daly, K. P., Matusz, P., Tubbs, R. S., & Loukas, M. (2014). Anatomical significance in aortoiliac occlusive disease. *Clinical Anatomy*, 27(8),1264–1274. https://doi.org/10.1002/ca.22444

Zhao, Y., Ping, J., Yu, X., Wu, R., Sun, C., & Zhang, M. (2019). Fractional flow reserve-based 4d hemodynamic simulation of time-resolved blood flow in left anterior descending coronary artery. *Clinical Biomechanics*, 70, 164–169. https://doi.org/10.1016/j.clinbiomech.2019.09.003

Zhu, C., Seo, J. H., & Mittal, R. (2018). Computational modelling and analysis of haemodynamics in a simple model of aortic stenosis. *Journal of Fluid Mechanics*, 851, 23–49. https://doi.org/10.1017/jfm.2018.463